Noname manuscript No.
(will be inserted by the editor)

Mortar-based entropy stable discontinuous Galerkin methods on non-conforming quadrilateral and hexahedral meshes

Jesse Chan, Mario Bencomo, David C. Del Rey Fernandez

Abstract High order entropy stable discontinuous Galerkin (DG) methods for nonlinear conservation laws reproduce a discrete entropy inequality by combining entropy conservative finite volume fluxes with summation-by-parts (SBP) discretization matrices. On tensor product (quadrilateral and hexahedral) elements, SBP matrices are typically constructed by collocating at Lobatto quadrature points. Recent work has extended the construction of entropy stable DG schemes to collocation at more accurate Gauss quadrature points [1].

In this work, we extend entropy stable Gauss collocation schemes to non-conforming meshes. Entropy stable DG schemes require computing entropy conservative numerical fluxes between volume and surface quadrature nodes. On conforming tensor product meshes where volume and surface nodes are aligned, flux evaluations are required only between "lines" of nodes. However, on non-conforming meshes, volume and surface nodes are no longer aligned, resulting in a larger number of flux evaluations. We reduce this expense by introducing an entropy stable mortar-based treatment of non-conforming interfaces via a face-local correction term, and provide truncation error estimates for the resulting discretizations. Numerical experiments confirm the stability and accuracy of this approach, and we conclude by discussing how to extend mortar treatments of non-conforming interfaces to general elements and arbitrary quadrature rules [2].

1 Introduction

Discretely entropy stability has emerged as a methodology for designing high order schemes for nonlinear conservation laws. Entropy stable discretizations ensure the satisfaction of a semi-discrete entropy inequality by combining specific finite volume numerical fluxes with summation-by-parts (SBP) discretization matrices. Compared to traditional high order methods, the resulting schemes demonstrate significantly improved robustness in the presence of under-resolved solution features such as shocks or turbulence while retaining high order accuracy.

Entropy stable discontinuous Galerkin (DG) methods were originally constructed for quadrilateral and hexahedral meshes based on nodal collocation at

Address(es) of author(s) should be given

Lobatto quadrature points [3–5]. Entropy stable schemes were later extended to simplicial and more general elements using tailored volume and surface quadrature rules [6, 7]. More general quadrature rules were addressed in [1, 2, 8, 9], including entropy stable collocation schemes on quadrilateral and hexahedral elements based on more accurate Gauss quadrature rules and generalized SBP operators [1].

The work presented here focuses on geometrically non-conforming meshes. Such meshes may arise when applying domain decomposition techniques to a complex geometry (e.g. meshing sub-domains independently) [10] or performing local mesh refinement. Entropy stable Lobatto collocation schemes have been constructed on non-conforming meshes in [11] using SBP projection operators. In this work, we extend entropy stable Gauss collocation to non-conforming quadrilateral and hexahedral meshes. While it is straightforward to construct Gauss collocation schemes on non-conforming meshes, the treatment of non-conforming interfaces results in signficantly increased computational costs. We reduce such costs by adopting a mortar-based treatment of non-conforming interfaces. Moreover, while the cost of the proposed scheme is similar to that of [11] in 2D, the mortar-based approach is more computationally efficient for both Lobatto and Gauss collocation schemes on 3D non-conforming hexahedral meshes.

The paper is organized as follows: Section 2 briefly reviews the derivation of an entropy inequality for a system of nonlinear conservation laws. Section 3 introduces "hybridized" SBP operators as a unified way to treat both Lobatto and Gauss collocation schemes on conforming meshes of tensor product elements. Section 4 describes a naive extension to non-conforming meshes and illustrates why this formulation results in an increase in computational costs. Section 5 introduces a mortar-based formulation which addresses such costs, and characterizes the accuracy of the resulting formulations. Section **??** describes the extension to curved meshes, as well as more general elements and p non-conformity. We conclude with numerical validation of theoretical results in Section **??**.

2 Entropy stability for systems of nonlinear conservation laws

We are interested in the numerical approximation of solutions to systems of nonlinear conservation laws

$$\frac{\partial \boldsymbol{u}}{\partial t} + \sum_{i=1}^{d} \frac{\partial \boldsymbol{f}_i(\boldsymbol{u})}{\partial x_i} = 0. \tag{1}$$

Here, $\boldsymbol{u}$ denotes the conservative variables and $\boldsymbol{f}_i(\boldsymbol{u})$ are nonlinear fluxes. We briefly review entropy stability for systems of conservation laws in d dimensions. We assume there exists a convex scalar entropy $S(\boldsymbol{u})$ associated with (1). We then define the entropy variables $\boldsymbol{v}(\boldsymbol{u})$ as the gradient of the entropy $S(\boldsymbol{u})$ with respect to the conservative variables

$$\boldsymbol{v} = \frac{\partial S(\boldsymbol{u})}{\partial \boldsymbol{u}}.$$

For $S(\boldsymbol{u})$ convex, $\boldsymbol{v}(\boldsymbol{u})$ defines an invertible mapping between the conservative and entropy variables, whose inverse (from entropy to conservative variables) we denote by $\boldsymbol{u}(\boldsymbol{v})$. Viscosity solutions to (1) satisfy an integrated form of the entropy

inequality [12]

$$\int_\Omega \frac{\partial S(\boldsymbol{u})}{\partial t} + \int_{\partial\Omega} \sum_{i=1}^{d} \boldsymbol{n}_i \left(\boldsymbol{v}^T \boldsymbol{f}_i(\boldsymbol{u}) - \psi_i(\boldsymbol{u}) \right) \leq 0, \tag{2}$$

where F_i denotes the ith scalar entropy flux function, $\psi_i(\boldsymbol{u}) = \boldsymbol{v}^T \boldsymbol{f}_i(\boldsymbol{u}) - F_i(\boldsymbol{u})$ denotes the ith entropy potential, $\partial\Omega$ denotes the boundary of Ω and $\boldsymbol{n}_i$ denotes the ith component of the outward normal on $\partial\Omega$. This can be interpreted as implying that the time rate of change of entropy is bounded by the entropy flux through the boundary.

3 Entropy stable collocation DG methods and hybridized SBP operators

In this section, we summarize the work of [1] on the construction of entropy stable collocation DG methods based on generalized summation by parts (GSBP) operators. These constructions are applicable to collocation schemes based on either Lobatto and Gauss nodes.

3.1 Hybridized SBP operators in 1D

We begin by introducing collocation discretization matrices on the reference interval $[-1, 1]$. We assume the solution is collocated at $(N+1)$ quadrature points x_i with associated quadrature weights w_i, and consider primarily Lobatto or Gauss quadrature points. The collocation assumption is equivalent to approximating the solution using a degree N Lagrange basis $\ell_j(x)$ at the $(N+1)$ quadrature points.

We define mass and integrated differentiation matrices $\boldsymbol{M}, \boldsymbol{Q}$

$$\boldsymbol{M}_{ij} = \int_{-1}^{1} \ell_i(x)\ell_j(x), \qquad \boldsymbol{Q}_{ij} = \int_{-1}^{1} \frac{\partial \ell_j}{\partial x} \ell_i.$$

We assume that all integrals are computed using the collocated quadrature rule, such that

$$\begin{aligned} \boldsymbol{M}_{ij} &= \int_{-1}^{1} \ell_i(x)\ell_j(x) \approx \sum_{k=1}^{N+1} \ell_i(x_k)\ell_j(x_k)w_k = \delta_{ij} w_i \\ \boldsymbol{Q}_{ij} &= \int_{-1}^{1} \frac{\partial \ell_j}{\partial x} \ell_i \approx \sum_{k=1}^{N+1} \ell_i(x_k) \left.\frac{\partial \ell_j}{\partial x}\right|_{x_k} w_k. \end{aligned}$$

In other words, the mass matrix is diagonal with entries equal to the quadrature weights. Since the integrands of $\boldsymbol{M}$ are degree $2N$ polynomials, the collocation approximation of $\boldsymbol{M}$ is exact for Gauss quadrature, but not for Lobatto quadrature. For both Gauss and Lobatto quadrature, the matrix $\boldsymbol{Q}$ is exact under collocation quadrature.

We introduce the $2 \times (N+1)$ matrix $\boldsymbol{E}$ which interpolates values at collocation nodes to values at the endpoints $x = -1$ and $x = 1$. These two matrices are defined entrywise as

$$(\boldsymbol{E})_{1i} = \ell_i(-1), \qquad (\boldsymbol{E})_{2i} = \ell_i(1).$$

The mass and differentiation matrices satisfy a generalized summation by parts property [13]

$$\boldsymbol{Q} = \boldsymbol{E}^T \boldsymbol{B} \boldsymbol{E} - \boldsymbol{Q}^T, \qquad \boldsymbol{B} = \begin{bmatrix} -1 & \\ & 1 \end{bmatrix}. \tag{3}$$

The GSBP property holds for both Lobatto and Gauss nodes, and switching between these two nodal sets simply requires redefining the matrices $\boldsymbol{D}, \boldsymbol{E}$. For Gauss nodes, $\boldsymbol{E}$ is dense. For Lobatto nodes, since the collocation nodes include boundary points, the interpolation matrix $\boldsymbol{E}$ reduces to the matrix which extracts nodal values associated with the left and right endpoints

$$\boldsymbol{E} = \begin{bmatrix} 1 & 0 & \dots & 0 \\ 0 & \dots & 0 & 1 \end{bmatrix}.$$

It is possible to construct energy stable high order discretizations of linear hyperbolic systems using GSBP operators based on Gauss nodes [13]. However, for nonlinear conservation laws, the presence of the dense $\boldsymbol{E}$ matrix in the GSBP property (3) complicates the imposition of boundary conditions and computation of inter-element numerical fluxes [1, 2, 7]. This can be avoided by using "hybridized" (or decoupled) SBP operators [2, 9, 14], which are defined as the block matrix

$$\boldsymbol{Q}_h = \frac{1}{2} \begin{bmatrix} \boldsymbol{Q} - \boldsymbol{Q}^T & \boldsymbol{E}^T \boldsymbol{B} \\ -\boldsymbol{B}\boldsymbol{E} & \boldsymbol{B} \end{bmatrix}.$$

The hybridized SBP operator satisfies a block form of the SBP property

$$\boldsymbol{Q}_h + \boldsymbol{Q}_h^T = \boldsymbol{B}_h, \qquad \boldsymbol{B}_h = \begin{bmatrix} \boldsymbol{0} & \\ & \boldsymbol{B} \end{bmatrix}. \tag{4}$$

where $\boldsymbol{E}$ does not appear in the block boundary matrix on the right hand side. Here, we have used $\boldsymbol{0}, \boldsymbol{1}$ to denote a matrix or vector of zeros or ones, where the size is inferred from context. Note that the matrix $\boldsymbol{Q}_h$ also satisfies

$$\boldsymbol{Q}_h \boldsymbol{1} = \frac{1}{2} \begin{bmatrix} \boldsymbol{Q}\boldsymbol{1} - \boldsymbol{Q}^T \boldsymbol{1} + \boldsymbol{E}^T \boldsymbol{B} \boldsymbol{1} \\ -\boldsymbol{B}\boldsymbol{E}\boldsymbol{1} - \boldsymbol{B}\boldsymbol{1} \end{bmatrix} = \frac{1}{2} \begin{bmatrix} \left(-\boldsymbol{Q}^T + \boldsymbol{E}^T \boldsymbol{B}\right) \boldsymbol{1} \\ \boldsymbol{0} \end{bmatrix} = \frac{1}{2} \begin{bmatrix} \boldsymbol{Q}\boldsymbol{1} \\ \boldsymbol{0} \end{bmatrix} = \boldsymbol{0} \tag{5}$$

where we have used that $\boldsymbol{E}\boldsymbol{1} = \boldsymbol{1}$ (since $\boldsymbol{E}$ is a high order accurate boundary interpolation matrix), $\boldsymbol{Q}\boldsymbol{1} = \boldsymbol{0}$ (since $\boldsymbol{Q}$ is a differentiation matrix), and the GSBP property $-\boldsymbol{Q}^T + \boldsymbol{E}^T \boldsymbol{B} \boldsymbol{E} = \boldsymbol{Q}$

3.2 Hybridized SBP operators in higher dimensions

The formulation (2) can be extended to higher dimensions through a tensor product construction. For simplicity, we illustrate this for 2D quadrilateral elements (the extension to 3D hexahedral elements is straightforward). Let $\boldsymbol{M}_{1\mathrm{D}}, \boldsymbol{Q}_{1\mathrm{D}}$ denote one-dimensional generalized SBP norm (mass) and differentiation matrices, and let $\boldsymbol{E}_{1\mathrm{D}}$ denote the 1D face interpolation matrix. We define multi-dimensional mass and differentiation matrices in terms of Kronecker products

$$\widehat{\boldsymbol{Q}}_1 = \boldsymbol{Q}_{1\mathrm{D}} \otimes \boldsymbol{M}_{1\mathrm{D}}, \qquad \widehat{\boldsymbol{Q}}_2 = \boldsymbol{M}_{1\mathrm{D}} \otimes \boldsymbol{Q}_{1\mathrm{D}}, \qquad \widehat{\boldsymbol{M}} = \boldsymbol{M}_{1\mathrm{D}} \otimes \boldsymbol{M}_{1\mathrm{D}}. \tag{6}$$

We also construct 2D face interpolation matrices from Kronecker products. Let $\boldsymbol{E}_{1\mathrm{D}}$ denote the one-dimensional face interpolation matrix, and let $\boldsymbol{B}_{1\mathrm{D}}$ denote the 1D boundary matrix in (3). For a specific ordering of the face points, the two-dimensional face interpolation matrix $\boldsymbol{E}$ and reference boundary matrices $\widehat{\boldsymbol{B}}_1, \widehat{\boldsymbol{B}}_2$ are given by

$$\boldsymbol{E} = \begin{bmatrix} \boldsymbol{E}_{1\mathrm{D}} \otimes \boldsymbol{I}_2 \\ \boldsymbol{I}_2 \otimes \boldsymbol{E}_{1\mathrm{D}} \end{bmatrix}, \qquad \widehat{\boldsymbol{B}}_1 = \begin{bmatrix} \boldsymbol{B}_{1\mathrm{D}} \otimes \boldsymbol{M}_{1\mathrm{D}} & \\ & \boldsymbol{0} \end{bmatrix}, \qquad \widehat{\boldsymbol{B}}_2 = \begin{bmatrix} \boldsymbol{0} & \\ & \boldsymbol{M}_{1\mathrm{D}} \otimes \boldsymbol{B}_{1\mathrm{D}} \end{bmatrix}, \tag{7}$$

where $\boldsymbol{I}_2$ is the 2×2 identity matrix. Recall that $\boldsymbol{M}_{1\mathrm{D}}$ is the diagonal matrix of quadrature weights, so $\widehat{\boldsymbol{B}}_i$ are diagonal.

The construction of operators in (6) and (7) correspond to the use of tensor product points quadrature points and *aligned* surface points. For example, if Gauss points are used for volume quadrature, we assume that Gauss points are also used for surface quadrature. This ensures that the operators $\widehat{\boldsymbol{Q}}_i, \widehat{\boldsymbol{B}}_i, \boldsymbol{E}$ satisfy the analogous higher dimensional generalized SBP property $\widehat{\boldsymbol{Q}}_i = \boldsymbol{E}^T \widehat{\boldsymbol{B}}_i \boldsymbol{E} - \widehat{\boldsymbol{Q}}_i^T$.

The 2D differentiation and interpolation matrices $\widehat{\boldsymbol{Q}}_i, \boldsymbol{E}$ can now be used to construct 2D hybridized SBP operators. Let $\widehat{\boldsymbol{Q}}_{i,h}$ denote the hybridized SBP operator for the ith coordinate on the reference element, where $\widehat{\boldsymbol{Q}}_{i,h}$ is defined as

$$\widehat{\boldsymbol{Q}}_{i,h} = \frac{1}{2} \begin{bmatrix} \widehat{\boldsymbol{Q}}_i - \widehat{\boldsymbol{Q}}_i^T & \boldsymbol{E}^T \widehat{\boldsymbol{B}}_i \\ -\widehat{\boldsymbol{B}}_i \boldsymbol{E} & \widehat{\boldsymbol{B}}_i \end{bmatrix}. \tag{8}$$

These matrices satisfy the following multi-dimensional properties:

Lemma 1 *Let $\widehat{\boldsymbol{Q}}_i$ be defined as in (6) and let $\widehat{\boldsymbol{Q}}_{i,h}$ be defined as in (8). Then,*

$$\widehat{\boldsymbol{Q}}_{i,h} + \widehat{\boldsymbol{Q}}_{i,h}^T = \begin{bmatrix} \boldsymbol{0} & \\ & \widehat{\boldsymbol{B}}_i \end{bmatrix}, \qquad \widehat{\boldsymbol{Q}}_{i,h} \boldsymbol{1} = \boldsymbol{0}. \tag{9}$$

The proof is contained in [1]. The SBP property follows from the construction of $\widehat{\boldsymbol{Q}}_{i,h}$, and $\widehat{\boldsymbol{Q}}_{i,h}\boldsymbol{1} = \boldsymbol{0}$ is a consequence of the Kronecker product and the same arguments used to derive (5). The construction of 3D differentiation and interpolation matrices proceeds similarly, and the matrices satisfy the same properties as described in Lemma 1.

We now construct an entropy conservative formulation on an unstructured curved mesh. Suppose the domain Ω is decomposed into non-overlapping elements D^k which are images of the reference mapping, such that D^k is a differentiable mapping of the reference element $\widehat{D} = [-1, 1]^d$. Let $\boldsymbol{x}_i$ denote the ith physical coordinate on D^k and let $\widehat{\boldsymbol{x}}_j$ denote the jth reference coordinate. The mapping between reference and physical element induces scaled geometric terms

$$G_{ij} = J \frac{\partial \widehat{\boldsymbol{x}}_j}{\partial \boldsymbol{x}_i},$$

where J denotes the determinant of the Jacobian of the physical-to-reference mapping. We refer to J as the Jacobian from here onwards. These geometric terms also relate the normal vectors on reference and physical elements. Let $\widehat{\boldsymbol{n}}\widehat{J}_f$ denote the outward normal vector on $\widehat{D}$, scaled by the reference face Jacobians. Then, the (scaled) physical normal vectors on D^k are related to $\widehat{\boldsymbol{n}}\widehat{J}_f$ through

$$n_i J_f = \sum_{j=1}^{d} G_{ij} \widehat{n}_j \widehat{J}_f. \tag{10}$$

We assume that the mesh is watertight, such that the scaled normal vectors are equal and opposite across shared faces between two elements. We also assume that the geometric terms G_{ij} are constructed such that they are polynomials of degree less than or equal to N and satisfy a discrete geometric conservation law (GCL)

$$\sum_{j=1}^{d} \frac{\partial}{\partial \widehat{x}_j} G_{ij} = 0. \tag{11}$$

The discrete GCL is satisfied automatically for isoparametric mappings in 2D, and there exist several techniques to enforce the satisfaction of a discrete GCL on various three-dimensional domains [7, 8, 15–18].

We can now assemble physical mass and differentiation matrices on D^k from reference mass and differentiation matrices using the chain rule. Let $\widehat{\boldsymbol{Q}}_{j,h}$ denote the jth reference differentiation matrix on $\widehat{D}$. We can define the physical differentiation matrices $\boldsymbol{Q}_{i,h}$ on D^k via the skew-symmetric splitting

$$\boldsymbol{Q}_{i,h} = \frac{1}{2} \sum_{j=1}^{d} \operatorname{diag}\left(\boldsymbol{G}_{ij}\right) \widehat{\boldsymbol{Q}}_{j,h} + \widehat{\boldsymbol{Q}}_{j,h} \operatorname{diag}\left(\boldsymbol{G}_{ij}\right), \tag{12}$$

where $\boldsymbol{G}_{ij}$ denotes the vector of values of $G_{ij} = J \frac{\partial \widehat{\boldsymbol{x}}_j}{\partial \boldsymbol{x}_i}$ at both volume and surface points. Since G_{ij} is assumed to be a polynomial of degree less than or equal to N, $\boldsymbol{G}_{ij}$ is constructed using polynomial interpolation.

Because the reference matrices $\widehat{\boldsymbol{Q}}_{j,h}$ satisfy the reference SBP properties (4), one can show [8] that the physical matrices $\boldsymbol{Q}_{i,h}$ satisfy analogous SBP properties.

Lemma 2 *Suppose the geometric terms $\boldsymbol{G}_{ij}$ satisfy the discrete GCL (11), the normals are constructed via (10), and that $\boldsymbol{Q}_{i,h}$ is constructed using (12). Then,*

$$\boldsymbol{Q}_{i,h} + \boldsymbol{Q}_{i,h}^T = \begin{bmatrix} \boldsymbol{0} & \\ & \boldsymbol{B}_i \end{bmatrix}, \qquad \boldsymbol{Q}_{i,h} \boldsymbol{1} = \boldsymbol{0},$$

where $\boldsymbol{n}_i$ is a vector whose entries are values of the ith component of the scaled normals $n_i J_f$ at face points, $\boldsymbol{w}_f$ is the vector of face quadrature weights w_i, and $\boldsymbol{B}_i = \operatorname{diag}\left(\boldsymbol{n}_i \circ \boldsymbol{w}_f\right)$.

Proof The proof is identical to that of [8]. We review it here for completeness. Expanding out $\boldsymbol{Q}_{i,h} + \boldsymbol{Q}_{i,h}^T$ yields

$$\frac{1}{2} \sum_{j=1}^{d} \operatorname{diag}\left(\boldsymbol{G}_{ij}\right) \widehat{\boldsymbol{Q}}_{j,h} + \widehat{\boldsymbol{Q}}_{j,h}^T \operatorname{diag}\left(\boldsymbol{G}_{ij}\right) + \widehat{\boldsymbol{Q}}_{j,h} \operatorname{diag}\left(\boldsymbol{G}_{ij}\right) + \operatorname{diag}\left(\boldsymbol{G}_{ij}\right) \widehat{\boldsymbol{Q}}_{j,h}^T.$$

For each term in the sum, we apply the SBP property of $\widehat{\boldsymbol{Q}}_{j,h}$. The volume terms cancel, leaving only surface terms

$$\frac{1}{2} \sum_{j=1}^{d} \left(\widehat{\boldsymbol{B}}_{j,h} \operatorname{diag}\left(\boldsymbol{G}_{ij}\right) + \operatorname{diag}\left(\boldsymbol{G}_{ij}\right) \widehat{\boldsymbol{B}}_{j,h} \right) = \begin{bmatrix} \boldsymbol{0} & \\ & \boldsymbol{B}_i \end{bmatrix}.$$

where we have used (10) and that $\widehat{\boldsymbol{B}}_{j,h}$ and $\operatorname{diag}\left(\boldsymbol{G}_{ij}\right)$ are diagonal matrices.

To show $\boldsymbol{Q}_{i,h}\mathbf{1} = \mathbf{0}$, we note that

$$\boldsymbol{Q}_{i,h}\mathbf{1} = \frac{1}{2}\sum_{j=1}^{d} \operatorname{diag}\left(\boldsymbol{G}_{ij}\right)\widehat{\boldsymbol{Q}}_{j,h}\mathbf{1} + \widehat{\boldsymbol{Q}}_{j,h}\operatorname{diag}\left(\boldsymbol{G}_{ij}\right)\mathbf{1} = \frac{1}{2}\sum_{j=1}^{d}\widehat{\boldsymbol{Q}}_{j,h}\boldsymbol{G}_{ij}$$

since $\widehat{\boldsymbol{Q}}_{j,h}\mathbf{1} = \mathbf{0}$ by Lemma 1. Note that, since $\boldsymbol{G}_{ij}$ is constructed using polynomial interpolation, $\boldsymbol{G}_{ij} = \left[G_{ij}(\widehat{\boldsymbol{x}}), \quad \boldsymbol{E}G_{ij}(\widehat{\boldsymbol{x}})\right]^T$, where $G_{ij}(\widehat{\boldsymbol{x}})$ denotes the values of G_{ij} at volume points. The remaining term can be expanded out

$$\begin{aligned}\sum_{j=1}^{d}\widehat{\boldsymbol{Q}}_{j,h}\boldsymbol{G}_{ij} &= \sum_{j=1}^{d}\begin{bmatrix}\widehat{\boldsymbol{Q}}_j G_{ij}(\widehat{\boldsymbol{x}}) - \widehat{\boldsymbol{Q}}_j^T G_{ij}(\widehat{\boldsymbol{x}}) + \boldsymbol{E}^T\boldsymbol{B}\boldsymbol{E}G_{ij}(\widehat{\boldsymbol{x}}) \\ \boldsymbol{B}\boldsymbol{E}G_{ij}(\widehat{\boldsymbol{x}}) - \boldsymbol{B}\boldsymbol{E}G_{ij}(\widehat{\boldsymbol{x}})\end{bmatrix} \\ &= \sum_{j=1}^{d}\begin{bmatrix}\left(-\widehat{\boldsymbol{Q}}_j^T + \boldsymbol{E}^T\boldsymbol{B}\boldsymbol{E}\right)G_{ij}(\widehat{\boldsymbol{x}}) \\ \mathbf{0}\end{bmatrix} = \sum_{j=1}^{d}\begin{bmatrix}\widehat{\boldsymbol{Q}}_j G_{ij}(\widehat{\boldsymbol{x}}) \\ \mathbf{0}\end{bmatrix} = \mathbf{0},\end{aligned}$$

where we have used the generalized SBP property and that $\sum_{j=1}^{d}\widehat{\boldsymbol{Q}}_j G_{ij}(\widehat{\boldsymbol{x}}) = \mathbf{0}$, since G_{ij} satisfies the discrete GCL (11), $G_{ij}(\widehat{\boldsymbol{x}})$ is a polynomial of degree less than or equal to N, and $\widehat{\boldsymbol{Q}}_j$ exactly differentiates polynomials of degree N. □

3.3 Entropy conservative formulations on conforming meshes of mapped elements

The aforementioned matrices can now be used to construct high order accurate entropy stable and entropy conservative schemes. We first introduce an entropy conservative numerical flux [19]. Let $\boldsymbol{u}_L, \boldsymbol{u}_R$ denote left and right states in the conservative variables. Then, an entropy conservative numerical flux is a vector-valued function $\boldsymbol{f}_{i,S}$ for $i = 1, \ldots, d$ which satisfies the following three properties

$$\begin{aligned}\boldsymbol{f}_{i,S}\left(\boldsymbol{u},\boldsymbol{u}\right) &= \boldsymbol{f}_i(\boldsymbol{u}), && \text{(consistency)} \\ \boldsymbol{f}_{i,S}\left(\boldsymbol{u}_L,\boldsymbol{u}_R\right) &= \boldsymbol{f}_{i,S}(\boldsymbol{u}_R,\boldsymbol{u}_L), && \text{(symmetry)} \\ \left(\boldsymbol{v}_L - \boldsymbol{v}_R\right)^T\boldsymbol{f}_{i,S}\left(\boldsymbol{u}_L,\boldsymbol{u}_R\right) &= \psi_i(\boldsymbol{u}_L) - \psi_i(\boldsymbol{u}_R), && \text{(conservation)}.\end{aligned}$$

Here, $\boldsymbol{v}_L, \boldsymbol{v}_R$ are the entropy variables evaluated at $\boldsymbol{u}_L, \boldsymbol{u}_R$, and ψ_i is the ith entropy potential which appears in (2). Then, an entropy conservative scheme on a mapped element is given by

$$\begin{aligned}\boldsymbol{M}\frac{\mathrm{d}\boldsymbol{u}_h}{\mathrm{d}t} + \begin{bmatrix}\boldsymbol{I} \\ \boldsymbol{E}\end{bmatrix}^T\sum_{i=1}^{d}\left(2\boldsymbol{Q}_{i,h}\circ\boldsymbol{F}_i\right)\mathbf{1} + \boldsymbol{E}^T\boldsymbol{B}_i\left(\boldsymbol{f}_i^* - \boldsymbol{f}_i(\widetilde{\boldsymbol{u}}_f)\right) = 0 \qquad (13)\\ \left(\boldsymbol{F}_i\right)_{jk} = \boldsymbol{f}_S\left(\widetilde{\boldsymbol{u}}_j,\widetilde{\boldsymbol{u}}_k\right), \qquad \boldsymbol{f}_i^* = \boldsymbol{f}_{i,S}\left(\widetilde{\boldsymbol{u}}_f^+,\widetilde{\boldsymbol{u}}_f\right)\end{aligned}$$

Here, the exterior state $\widetilde{\boldsymbol{u}}_f^+$ used to evaluate the numerical flux $\boldsymbol{f}_i^*$ corresponds either to interface values on a neighboring element or an exterior state used to enforce boundary conditions, and $\circ$ denotes the matrix Hadamard product.

Theorem 1 *Assuming continuity in time, the formulation (13) is entropy conservative in the sense that*

$$\mathbf{1}^T\boldsymbol{M}\frac{\mathrm{d}S(\boldsymbol{u}_h)}{\mathrm{d}t} + \sum_{i=1}^{d}\mathbf{1}^T\boldsymbol{B}_i\left(\boldsymbol{v}_f^T\boldsymbol{f}_i^* - \psi_i(\widetilde{\boldsymbol{u}}_f)\right) = 0, \qquad \boldsymbol{v}_f = \boldsymbol{E}\boldsymbol{v}(\boldsymbol{u}_h).$$

Proof The proof uses similar techniques as proofs in other papers [2, 6, 7, 9], and we repeat it for completeness. We begin by testing (13) with the vector of entropy variables evaluated at nodal points $\boldsymbol{v}(\boldsymbol{u}_h)$. We apply the chain rule in time and use that $\boldsymbol{M}$ is diagonal to show that

$$\boldsymbol{v}(\boldsymbol{u}_h)^T \boldsymbol{M} \frac{\mathrm{d}\boldsymbol{u}}{\mathrm{dt}} = \mathbf{1}^T \boldsymbol{M} \left(\boldsymbol{v}(\boldsymbol{u}_h) \circ \frac{\mathrm{d}\boldsymbol{u}_h}{\mathrm{dt}} \right) = \mathbf{1}^T \boldsymbol{M} \frac{\mathrm{d}S(\boldsymbol{u}_h)}{\mathrm{dt}}.$$

For the volume term, we use the SBP property to arrive at

$$\begin{aligned} &\boldsymbol{v}(\boldsymbol{u}_h)^T \begin{bmatrix} \boldsymbol{I} \\ \boldsymbol{E} \end{bmatrix}^T \left(2\boldsymbol{Q}_{i,h} \circ \boldsymbol{F}_i\right) \mathbf{1} = \\ &\widetilde{\boldsymbol{v}}^T \left(\left(\boldsymbol{Q}_{i,h} - \boldsymbol{Q}_{i,h}^T \right) \circ \boldsymbol{F}_i \right) \mathbf{1} + \left(\boldsymbol{E}\boldsymbol{v}(\boldsymbol{u}_h)\right)^T \left(\boldsymbol{B}_{i,h} \circ \boldsymbol{F}_i \right) \mathbf{1}, \end{aligned}$$

where we have introduced $\widetilde{\boldsymbol{v}} = \left(\begin{bmatrix} \boldsymbol{I} \\ \boldsymbol{E} \end{bmatrix} \boldsymbol{v}(\boldsymbol{u}_h) \right)$. Note that, by the consistency of the entropy conservative flux $\boldsymbol{f}_{i,S}$, the diagonal of $\boldsymbol{F}_i$ is the vector $\boldsymbol{f}_i(\widetilde{\boldsymbol{u}}_f)$. Using that $\boldsymbol{B}_{i,h}$ is diagonal (with non-zero diagonal sub-block $\boldsymbol{B}_i$), the latter term reduces to

$$\left(\boldsymbol{E}\boldsymbol{v}(\boldsymbol{u}_h)\right)^T \left(\boldsymbol{B}_{i,h} \circ \boldsymbol{F}_i \right) \mathbf{1} = \boldsymbol{v}_f^T \boldsymbol{B}_i \boldsymbol{f}_i(\widetilde{\boldsymbol{u}}_f) = \mathbf{1}^T \boldsymbol{B}_i \left(\boldsymbol{v}_f^T \boldsymbol{f}_i(\widetilde{\boldsymbol{u}}_f) \right).$$

The final part of the proof uses that

$$\begin{aligned} \widetilde{\boldsymbol{v}}^T \left(\left(\boldsymbol{Q}_{i,h} - \boldsymbol{Q}_{i,h}^T \right) \circ \boldsymbol{F}_i \right) \mathbf{1} &= \sum_j \widetilde{\boldsymbol{v}}_j \left(\boldsymbol{Q}_{i,h} - \boldsymbol{Q}_{i,h}^T \right)_{jk} (\boldsymbol{F}_i)_{jk} \\ &= \sum_j (\boldsymbol{Q}_h)_{jk} \left(\widetilde{\boldsymbol{v}}_j - \widetilde{\boldsymbol{v}}_k \right)^T \boldsymbol{f}_{i,S} \left(\widetilde{\boldsymbol{u}}_j, \widetilde{\boldsymbol{u}}_k \right) \\ &= \sum_j (\boldsymbol{Q}_h)_{jk} \left(\psi(\widetilde{\boldsymbol{u}}_j) - \psi(\widetilde{\boldsymbol{u}}_k) \right) = \widetilde{\boldsymbol{u}}^T \boldsymbol{Q}_{i,h} \mathbf{1} - \mathbf{1}^T \boldsymbol{Q}_{i,h} \widetilde{\boldsymbol{u}} \end{aligned}$$

The term $\boldsymbol{Q}_{i,h}\mathbf{1} = \mathbf{0}$ by (5). The proof is completed by applying the SBP property (4) to the remaining term, which reduces to $-\mathbf{1}^T \boldsymbol{B}_{i,h} \widetilde{\boldsymbol{u}} = -\mathbf{1}^T \boldsymbol{B}_i \widetilde{\boldsymbol{u}_f}$. □

Note that the proof of entropy conservation relies mainly on Lemma 2, which states that $\boldsymbol{Q}_{i,h}$ is conservative (e.g., exact for constants) and satisfies the SBP property. Extensions to the non-conforming setting will utilize the same properties.

All entropy conservative schemes described here can be made entropy stable by introducing entropy dissipation through mechanisms such as physical or artificial viscosity [20, 21]. We introduce dissipation by incorporating a penalization term into the interface flux [22]. For example, Lax-Friedrichs dissipation can be added by modifying the interface flux term $\boldsymbol{B}_i \boldsymbol{f}_i^*$

$$\boldsymbol{B}_i \boldsymbol{f}_i^* \Longrightarrow \boldsymbol{B}_i \boldsymbol{f}_i^* - \frac{\lambda}{2} [\![\widetilde{\boldsymbol{u}}_f]\!], \qquad [\![\widetilde{\boldsymbol{u}}_f]\!] = \widetilde{\boldsymbol{u}}_f^+ - \widetilde{\boldsymbol{u}}_f,$$

where λ is an estimate of the maximum wave speed [2, 6].

For the remainder of this work, we will construct formulations and prove they are entropy conservative, with the understanding that they can be made entropy stable by incorporating an entropy dissipative penalty term.

4 Non-conforming meshes

Section 3 describes the construction of entropy stable schemes on geometrically conforming meshes, where each element shares at most one neighbor across a face. We extend the construction of stable schemes to meshes containing geometric non-conformity, where an element can share a face with two or more neighboring elements. To ensure stability, the coupling conditions imposed at this non-conforming face must be handled appropriately. For DG discretizations, this is most naturally achieved by combining composite quadrature rules on non-conforming faces with appropriate evaluations of volume terms [17]. However, for entropy stable schemes, the naive use of composite quadrature at non-conforming interfaces can significantly increase the computational cost.

For quad and hex elements under tensor product volume quadrature, the differentiation matrices are Kronecker products of 1D differentiation matrices and diagonal mass matrices, which result in sparse operators. As a result, flux evaluations are only required between "lines" of volume nodes [1, 4]. Flux evaluations also follow the sparsity pattern of the matrix $\boldsymbol{E}$, which maps from volume nodes to surface nodes. For Lobatto or Gauss collocation methods on conforming quadrilateral and hexahedral meshes, $\boldsymbol{E}$ is sparse if the surface quadrature nodes are aligned with volume quadrature nodes [1]. In such cases, flux evaluations are required only between lines of volume nodes and adjacent surface nodes, as shown in Figure 1a.

Composite quadrature rules on non-conforming meshes, however, are not aligned with volume nodes. Suppose that D^k is a quadrilateral element with two neighbors across each face, such that every face is non-conforming and utilizes a composite quadrature rule. The entropy conservative formulation (13) can be extended to the non-conforming case by redefining the interpolation matrix $\boldsymbol{E}$ as the matrix which interpolates from volume nodes to composite surface nodes. However, this version of $\boldsymbol{E}$ is fully dense, and evaluating the formulation (13) requires flux evaluations between each surface node and *all* volume nodes, as illustrated in Figure 1b. This greatly increases computational costs, especially at high orders of approximation.

5 Entropy stable mortar formulations

The goal of this work is to reduce computational costs for Gauss collocation schemes in the presence of non-conforming interfaces. This can be done by treating composite quadrature nodes as a layer of "mortar" nodes which are coupled directly to surface nodes, but not directly to the volume nodes, as illustrated in Figure 2. This results in modifications of the matrices involved in the entropy stable formulation (13). These modifications preserve both high order accuracy and entropy stablility, and yield an implementation which is identical to that of (13) except for a face-local correction to the numerical flux.

We introduce new matrices on the reference element $\widehat{D}$. Let $\widehat{\boldsymbol{x}}$ denote volume collocation points, and let $\widehat{\boldsymbol{x}}_f$ denote face (surface) points on the boundary $\partial\widehat{D}$. To simplify notation, we assume from this point onwards that the nodes are ordered face-by-face. In 2D, this implies that $\widehat{\boldsymbol{x}}_f$ is

$$\widehat{\boldsymbol{x}}_f = \left[\widehat{\boldsymbol{x}}_{f,1}\ \widehat{\boldsymbol{x}}_{f,2}\ \widehat{\boldsymbol{x}}_{f,3}\ \widehat{\boldsymbol{x}}_{f,4}\right]^T, \tag{14}$$

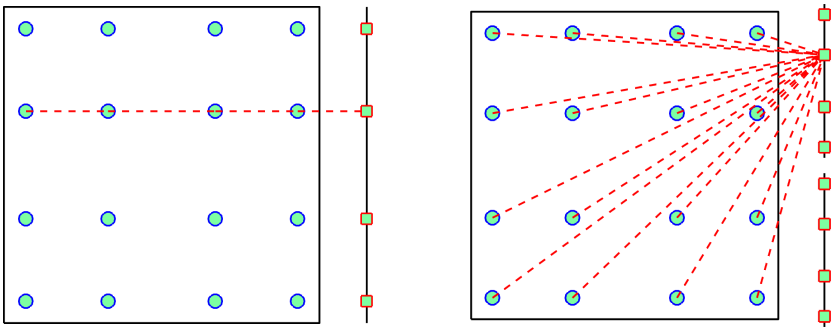

(a) Flux evaluations required for aligned surface nodes

(b) Flux evaluations required for non-aligned surface nodes

Fig. 1: Nodes between which flux evaluations are required for Gauss nodes. Aligned surface nodes (conforming interfaces) require evaluations between each surface node and a line of volume nodes, while non-aligned surface nodes (non-conforming interfaces) require flux evaluations between a surface node and *all* volume nodes.

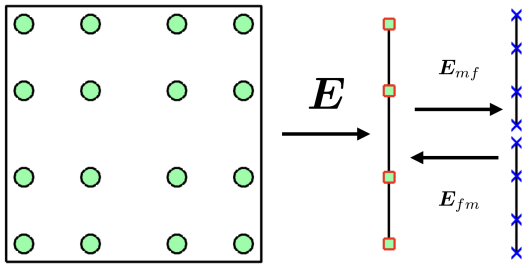

Fig. 2: Illustration of mortar operators for a Gauss collocation scheme. The matrix $\boldsymbol{E}$ maps from volume quadrature points to surface quadrature points, $\boldsymbol{E}_m$ maps from surface to mortar surface points, and $\widetilde{\boldsymbol{E}}_m$ maps from mortar surface points to surface points.

where $\widehat{\boldsymbol{x}}_{f,j}$ denotes the vector of 1D nodal positions on the jth face of the reference quadrilateral $[-1,1]^2$. Recall that the matrix $\boldsymbol{E}$ as defined in (7) interpolates from volume collocation points $\widehat{\boldsymbol{x}}$ to a specific ordering of the surface points $\widehat{\boldsymbol{x}}_f$. The ordering (14) simply corresponds to a permutation of the interpolation matrix $\boldsymbol{E}$.

We now introduce a second set of mortar points $\widehat{\boldsymbol{x}}_m$ on a face of the reference element. We assume these points also correspond to quadrature nodes with corresponding weights $\boldsymbol{w}_m$. For example, mortar nodes can be composite Gauss or Lobatto quadrature nodes (for h non-conforming interfaces), higher degree Gauss or Lobatto nodes (for p non-conforming interfaces), or identical to the surface nodes $\widehat{\boldsymbol{x}}_f$ (non-mortar interface). For simplicity of notation, we assume that each face has the same set of mortar nodes; however, it is straightforward to extend this to the case when the mortar nodes vary face-by-face.

We define the interpolation matrix $\boldsymbol{E}_{mf}$ as the operator which maps values at surface nodes to values at mortar nodes. In 2D, since the face of a quadrilateral is a 1D line, we can define $\boldsymbol{E}_{mf}$ as the block matrix acting on the surface nodes on the four faces

$$\boldsymbol{E}_{mf} = \boldsymbol{I}_{4\times 4} \otimes \boldsymbol{E}_m,$$

where $\boldsymbol{I}_{4\times 4}$ is the 4-by-4 identity matrix and $\boldsymbol{E}_m$ is the mortar interpolation matrix over the reference face (interval) $[-1, 1]$. The matrix $\boldsymbol{E}_m$ is defined in terms of $\widehat{x}_{m,i}$, the mortar nodes mapped to the reference interval $[-1, 1]$,

$$\boldsymbol{E}_{mf} = \ell_j(\widehat{x}_{m,i}), \qquad 1 \le i \le \text{num. mortar points}, \quad 1 \le j \le (N+1).$$

We can define an analogous matrix $\boldsymbol{E}_{fm}$ which maps from the mortar nodes back to the surface nodes. We first define the face mass matrix as the block diagonal matrix whose blocks are 1D diagonal mass matrices

$$\boldsymbol{M}_f = \boldsymbol{I}_{4\times 4} \otimes \boldsymbol{M}_{\text{1D}}.$$

These matrices are defined in 2D for simplicity, but are straightforward to extend to 3D. The matrix $\boldsymbol{E}_{fm}$ can now be defined through a quadrature-based L^2 projection

$$\boldsymbol{E}_{fm} = \boldsymbol{M}_f^{-1} \boldsymbol{E}_{mf}^T \boldsymbol{M}_m, \qquad \boldsymbol{M}_m = \boldsymbol{I}_{4\times 4} \otimes \operatorname{diag}(\boldsymbol{w}_m).$$

Finally, we introduce diagonal boundary matrices on surface and mortar nodes

$$\widehat{\boldsymbol{B}}_{i,f} = \operatorname{diag}\left(\widehat{\boldsymbol{n}}_{i,f}\right) \boldsymbol{M}_f \qquad \widehat{\boldsymbol{B}}_{i,m} = \operatorname{diag}\left(\widehat{\boldsymbol{n}}_{i,m}\right) \boldsymbol{M}_m, \tag{15}$$

where $\widehat{\boldsymbol{n}}_{i,f}, \widehat{\boldsymbol{n}}_{i,m}$ are vectors containing components of the scaled reference normals at face and mortar points, respectively.

Note that $\boldsymbol{E}_{fm}$ exactly recovers polynomials of a certain degree on the reference face, where the degree of the polynomial is related to the accuracy of the surface and mortar quadratures.

Lemma 3 *Suppose the face (surface) quadrature is exact for polynomials of degree $N + N_f$ and mortar quadratures are exact for degree $N + N_m$ polynomials. Then, $\boldsymbol{E}_{fm}$ exactly recovers polynomials of degree* $\min(N, N_f, N_m)$.

Proof Let $u(\boldsymbol{x})$ be a polynomial of degree $\min(N, N_f, N_m)$ or less, and let $\boldsymbol{u}_f$ be its values on the face (surface) nodes. Then, $\boldsymbol{u}_m = \boldsymbol{E}_{mf}\boldsymbol{u}_f$ are the interpolated values of the polynomial on the mortar nodes. Applying $\boldsymbol{E}_{fm}$ yields

$$\boldsymbol{E}_{fm}\boldsymbol{u}_m = \boldsymbol{M}_f^{-1}\boldsymbol{E}_{mf}^T\boldsymbol{M}_m\boldsymbol{E}_{mf}\boldsymbol{u}_f.$$

The entries of $\boldsymbol{E}_{mf}^T\boldsymbol{M}_m\boldsymbol{E}_{mf}$ are integrals of products of Lagrange basis functions with $u(\boldsymbol{x})$, where all integrals are approximated using mortar quadrature.

Since u is degree $\min(N, N_f, N_m)$ and each Lagrange basis function is degree N, the integrand is computed exactly under the mortar quadrature. Moreover, since u is degree $\min(N, N_f, N_m)$, it is also computed exactly using the face (surface) quadrature. Thus, $\boldsymbol{E}_{mf}^T\boldsymbol{M}_m\boldsymbol{E}_{mf}\boldsymbol{u}_f = \boldsymbol{M}_f\boldsymbol{u}_f$ by exactness of the face and mortar quadratures, and $\boldsymbol{E}_{fm}\boldsymbol{u}_m = \boldsymbol{u}_f$. □

5.1 Mortar-based hybridized SBP operators

The matrices $\boldsymbol{E}_{mf}, \boldsymbol{E}_{fm}, \widehat{\boldsymbol{B}}_{i,f}, \widehat{\boldsymbol{B}}_{i,m}$ can now be used to construct SBP operators which involve mortar nodes. We define the mortar-based hybridized SBP operator on the reference element $\widehat{\boldsymbol{Q}}_{i,m}$ to be

$$\widehat{\boldsymbol{Q}}_{i,m} = \frac{1}{2}\begin{bmatrix} \widehat{\boldsymbol{Q}}_i - \widehat{\boldsymbol{Q}}_i^T & \boldsymbol{E}^T\widehat{\boldsymbol{B}}_{i,f} & \\ -\widehat{\boldsymbol{B}}_{i,f}\boldsymbol{E} & & \widehat{\boldsymbol{B}}_{i,f}\boldsymbol{E}_{fm} \\ & -\widehat{\boldsymbol{B}}_{i,m}\boldsymbol{E}_{mf} & \widehat{\boldsymbol{B}}_{i,m} \end{bmatrix}. \tag{16}$$

Since it is not clear at first glance how the hybridized operator $\widehat{\boldsymbol{Q}}_{i,h}$ or its mortar-based variant $\widehat{\boldsymbol{Q}}_{i,m}$ can be used to perform differentiation, we review intuitive explanations of each operator.

Let $\boldsymbol{u}$ denote basis coefficients for some function $u(\boldsymbol{x})$, and let f, g denote two functions on the reference element. Suppose $\boldsymbol{u}$ satisfies the following matrix system involving the standard hybridized operator $\widehat{\boldsymbol{Q}}_{i,h}$

$$\widehat{\boldsymbol{M}}\boldsymbol{u} = \begin{bmatrix}\boldsymbol{I}\\ \boldsymbol{E}\end{bmatrix}^T \text{diag}\left(\boldsymbol{f}\right)\widehat{\boldsymbol{Q}}_{i,h}\text{diag}\left(\boldsymbol{g}\right), \qquad \boldsymbol{f} = \begin{bmatrix} f(\widehat{\boldsymbol{x}}) \\ f(\widehat{\boldsymbol{x}}_f)\end{bmatrix}, \qquad \boldsymbol{g} = \begin{bmatrix} g(\widehat{\boldsymbol{x}}) \\ g(\widehat{\boldsymbol{x}}_f)\end{bmatrix}. \tag{17}$$

It was shown in [2, 9] that this corresponds to a high order accurate approximation of $f\frac{\partial g}{\partial x_i}$. Let $\boldsymbol{v}$ denote basis coefficients for some arbitrary degree N polynomial test function. Expanding out the different blocks of (17) and using generalized summation by parts for $\widehat{\boldsymbol{Q}}_i$ yields

$$\widehat{\boldsymbol{M}}\boldsymbol{u} = \text{diag}\left(f(\widehat{\boldsymbol{x}})\right)\widehat{\boldsymbol{Q}}_i g(\widehat{\boldsymbol{x}}) + \frac{1}{2}\left(\text{diag}\left(f(\widehat{\boldsymbol{x}})\right)\boldsymbol{E}^T + \boldsymbol{E}^T f(\widehat{\boldsymbol{x}}_f)\right)\widehat{\boldsymbol{B}}_i\left(g(\widehat{\boldsymbol{x}}_f) - \boldsymbol{E}g(\widehat{\boldsymbol{x}})\right).$$

The latter expression can be interpreted as a boundary correction term. Since $\boldsymbol{E}$ is a high order accurate boundary interpolation operator, this correction term vanishes if g is a degree N polynomial.

The mortar-based hybridized SBP operator can be similarly interpreted as a high order differentiation operator. Recall that $\boldsymbol{E}_{mf}$ interpolates from face nodes to mortar nodes, and that $\boldsymbol{E}$ interpolates from volume nodes to face nodes. Thus, the matrix $\boldsymbol{E}_{mf}\boldsymbol{E}$ interpolates from volume nodes to mortar nodes. We can use this matrix to replicate (17) for the mortar-based operator $\widehat{\boldsymbol{Q}}_{i,m}$. Let $\boldsymbol{u}$ solve the following system

$$\widehat{\boldsymbol{M}}\boldsymbol{u} = \begin{bmatrix}\boldsymbol{I}\\ \boldsymbol{E}\\ \boldsymbol{E}_{mf}\boldsymbol{E}\end{bmatrix}^T \text{diag}\left(\boldsymbol{f}\right)\widehat{\boldsymbol{Q}}_{i,m}\text{diag}\left(\boldsymbol{g}\right), \qquad \boldsymbol{f} = \begin{bmatrix} f(\widehat{\boldsymbol{x}}) \\ f(\widehat{\boldsymbol{x}}_f) \\ f(\widehat{\boldsymbol{x}}_m)\end{bmatrix}, \quad \boldsymbol{g} = \begin{bmatrix} g(\widehat{\boldsymbol{x}}) \\ g(\widehat{\boldsymbol{x}}_f) \\ g(\widehat{\boldsymbol{x}}_m)\end{bmatrix}. \tag{18}$$

Expanding out terms yields a similar expression involving multiple correction terms

$$\begin{aligned}\widehat{\boldsymbol{M}}\boldsymbol{u} = &\ \text{diag}\left(f(\widehat{\boldsymbol{x}})\right)\widehat{\boldsymbol{Q}}_i g(\widehat{\boldsymbol{x}}) \\ &+ \frac{1}{2}\text{diag}\left(f(\widehat{\boldsymbol{x}})\right)\boldsymbol{E}^T\widehat{\boldsymbol{B}}_{i,f}\left(g(\widehat{\boldsymbol{x}}_f) - \boldsymbol{E}g(\widehat{\boldsymbol{x}})\right) \\ &+ \frac{1}{2}\boldsymbol{E}^T\text{diag}\left(f(\widehat{\boldsymbol{x}}_f)\right)\widehat{\boldsymbol{B}}_{i,f}\left(\boldsymbol{E}_{fm}g(\widehat{\boldsymbol{x}}_m) - \boldsymbol{E}g(\widehat{\boldsymbol{x}})\right) \\ &+ \frac{1}{2}\boldsymbol{E}^T\boldsymbol{E}_{mf}^T\text{diag}\left(f(\widehat{\boldsymbol{x}}_m)\right)\widehat{\boldsymbol{B}}_{i,m}\left(g(\widehat{\boldsymbol{x}}_m) - \boldsymbol{E}_{mf}g(\widehat{\boldsymbol{x}}_f)\right)\end{aligned} \tag{19}$$

We can show that these correction terms vanish for polynomial functions g.

Lemma 4 *Let $f(\boldsymbol{x}) = 1$ and suppose that the face (surface) quadrature is exact for polynomials of degree $N + N_f$ and mortar quadratures are exact for degree $N + N_m$ polynomials. Then, derivative approximations given by the equations (18) and (19) are exact if $g(\boldsymbol{x})$ is a degree $\min(N, N_f, N_m)$ polynomial.*

Proof Following [2], if $f = 1$ and $g(\boldsymbol{x})$ is a degree N polynomial, then (19) is exact if the correction terms vanish. The first and third correction terms are zero by the fact that $\boldsymbol{E}, \boldsymbol{E}_{mf}$ are degree N interpolation operators, and the second correction term vanishes since Lemma 3 implies that $\boldsymbol{E}_{fm}$ exactly recovers polynomials of degree $\min(N, N_f, N_m)$. □

Finally, we note that the mortar-based hybridized SBP operators satisfy a summation by parts property.

Lemma 5 *Let $\widehat{\boldsymbol{Q}}_{i,m}$ be defined as in (16). Then,*

$$\widehat{\boldsymbol{Q}}_{i,m} + \widehat{\boldsymbol{Q}}_{i,m}^T = \begin{bmatrix} \boldsymbol{0} & & \\ & \boldsymbol{0} & \\ & & \widehat{\boldsymbol{B}}_{i,m} \end{bmatrix}, \qquad \widehat{\boldsymbol{Q}}_{i,m}\boldsymbol{1} = \boldsymbol{0}.$$

Proof The SBP property holds if

$$\widehat{\boldsymbol{B}}_{i,f}\boldsymbol{E}_{fm} = (\widehat{\boldsymbol{B}}_{i,m}\boldsymbol{E}_{mf})^T = \boldsymbol{E}_{mf}^T\widehat{\boldsymbol{B}}_{i,m}, \tag{20}$$

where we have used that $\widehat{\boldsymbol{B}}_{i,m}$ is diagonal. Recall that $\boldsymbol{E}_{fm} = \boldsymbol{M}_f^{-1}\boldsymbol{E}_{mf}^T\boldsymbol{M}_m$. Then, by the definition of $\widehat{\boldsymbol{B}}_{i,m}, \widehat{\boldsymbol{B}}_{i,h}$ in (15), we have that

$$\widehat{\boldsymbol{B}}_{i,f}\boldsymbol{E}_{fm} = \operatorname{diag}\left(\widehat{\boldsymbol{n}}_{i,f}\right)\boldsymbol{M}_f\boldsymbol{M}_f^{-1}\boldsymbol{E}_{mf}^T\boldsymbol{M}_m = \operatorname{diag}\left(\widehat{\boldsymbol{n}}_{i,f}\right)\boldsymbol{E}_{mf}^T\boldsymbol{M}_m.$$

Then, since the scaled outward normals $\widehat{n}_i\widehat{J}_f$ are constant over each face of the reference element and $\boldsymbol{E}_{mf}, \boldsymbol{M}_m$ are block diagonal matrices (with each block corresponding to a face), $\operatorname{diag}\left(\widehat{\boldsymbol{n}}_{i,f}\right)$ commutes and

$$\operatorname{diag}\left(\widehat{\boldsymbol{n}}_{i,f}\right)\boldsymbol{E}_{mf}^T\boldsymbol{M}_m = \boldsymbol{E}_{mf}^T\boldsymbol{M}_m\operatorname{diag}\left(\widehat{\boldsymbol{n}}_{i,m}\right) = \boldsymbol{E}_{mf}^T\widehat{\boldsymbol{B}}_{i,m}.$$

□

5.2 Mortar-based entropy conservative formulations on mapped elements

We can extend the above scheme to mapped curvilinear elements by constructing physical mortar-based hybridized SBP operators in a manner akin to (12). Abusing notation, we use $\boldsymbol{G}_{ij}$ to now denote the vector containing values of $G_{ij} = J\frac{\partial\widehat{\boldsymbol{x}}_j}{\partial\boldsymbol{x}_i}$ at volume, surface, and mortar points. Then, we define physical operators $\boldsymbol{Q}_{i,m}$ via

$$\boldsymbol{Q}_{i,m} = \frac{1}{2}\sum_{j=1}^{d}\operatorname{diag}\left(\boldsymbol{G}_{ij}\right)\widehat{\boldsymbol{Q}}_{j,m} + \widehat{\boldsymbol{Q}}_{j,m}\operatorname{diag}\left(\boldsymbol{G}_{ij}\right). \tag{21}$$

Proofs of entropy conservation (e.g., for the formulation (13)) require that the hybridized SBP operators are conservative (e.g., exact for constants) and satisfy

the SBP property. Entropy conservation for mortar-based formulations on mapped elements will require similar properties. However, in contrast to hybridized SBP operators, conservation for mapped mortar-based operators requires additional constraints on the accuracy of surface and mortar quadratures relative to the polynomial degree of the geometric mapping.

We assume now that each geometric mapping from reference element $\widehat{D}$ to physical element D^k is a polynomial of degree N_{geo}. We also introduce the space of tensor product polynomials in d dimensions $Q^{N_1,\ldots,N_d}$ as

$$Q^{N_1,\ldots,N_d} = \left\{ \widehat{x}_1^{i_1} \widehat{x}_2^{i_2} \ldots \widehat{x}_d^{i_d}, \qquad 0 \leq i_k \leq N_k, \quad k = 1, \ldots, d. \right\}$$

We denote the isotropic tensor product space $Q^N = Q^{N,\ldots,N}$ for conciseness.

In [9], it was shown that the geometric terms G_{ij} are tensor product polynomials of specific degrees. For mapped quadrilateral elements, G_{ij} satisfy

$$\begin{aligned} G_{i1} &\in Q^{N_{\text{geo}},N_{\text{geo}}-1} \\ G_{i2} &\in Q^{N_{\text{geo}}-1,N_{\text{geo}}}. \end{aligned}$$

for $i = 1, 2$, and the geometric terms naturally satisfy the GCL condition (11).

For hexahedral elements, it is more challenging to construct geometric terms G_{ij} which satisfy the GCL while retaining high order accuracy. This is further complicated by the fact that we must take into account the polynomial degrees of G_{ij} when proving conservation for mortar-based SBP operators. We consider two approaches for computing hexahedral geometric terms in this work:

1. Approach 1: the construction of G_{ij} from [16], which yields

$$G_{ij} \in Q^{N_{\text{geo}}}, \qquad i, j = 1, 2, 3.$$

2. Approach 2: the construction of G_{ij} from [17] (Appendix C.3, see also Footnote 3 in [9]), which yields

$$\begin{aligned} G_{i1} &\in Q^{N_{\text{geo}},N_{\text{geo}}-1,N_{\text{geo}}-1} \\ G_{i2} &\in Q^{N_{\text{geo}}-1,N_{\text{geo}},N_{\text{geo}}-1} \\ G_{i3} &\in Q^{N_{\text{geo}}-1,N_{\text{geo}}-1,N_{\text{geo}}}, \qquad i = 1, 2, 3. \end{aligned}$$

These approaches are described in more detail in Appendix A.

Lemma 6 *Suppose D^k is a tensor product element element with tensor product surface quadratures and that $\boldsymbol{Q}_{i,m}$ is constructed using (21). Suppose also that the surface quadrature is exact for Q^{N+N_f}, the mortar quadrature is exact for Q^{N+N_m}. If*

1. *D^k is a quadrilateral element and $N_{\text{geo}} \leq \min(N, N_f + 1, N_m + 1)$, or*
2. *D^k is a hexahedral element, G_{ij} is constructed via Approach 1 [16], and $N_{\text{geo}} \leq \min(N, N_f, N_m)$, or*
3. *D^k is hexahedral element, G_{ij} is constructed via Approach 2 [17], and $N_{\text{geo}} \leq \min(N, N_f + 1, N_m + 1)$,*

then

$$\begin{aligned} \boldsymbol{Q}_{i,m} + \boldsymbol{Q}_{i,m}^T &= \boldsymbol{B}_{i,m}, \quad \textit{(SBP property)} \\ \boldsymbol{Q}_{i,m}\mathbf{1} &= \mathbf{0}, \quad \textit{(conservation)}. \end{aligned}$$

Proof Using the SBP property of $\widehat{\boldsymbol{Q}}_{i,m}$, proving the SBP property follows the same steps as the proof of Lemma 2. To show conservation, expanding out $\boldsymbol{Q}_{i,m}\mathbf{1}$ yields

$$\boldsymbol{Q}_{i,m}\mathbf{1} = \frac{1}{2}\sum_{j=1}^{d} \operatorname{diag}(\boldsymbol{G}_{ij})\,\widehat{\boldsymbol{Q}}_{j,m}\mathbf{1} + \widehat{\boldsymbol{Q}}_{j,m}\operatorname{diag}(\boldsymbol{G}_{ij})\,\mathbf{1} = \frac{1}{2}\sum_{j=1}^{d} \widehat{\boldsymbol{Q}}_{j,m}\boldsymbol{G}_{ij}$$

since $\widehat{\boldsymbol{Q}}_{j,m}\mathbf{1} = \mathbf{0}$ by Lemma 5. Expanding out remaining terms using (19) yields

$$\begin{aligned}\sum_{j=1}^{d} \widehat{\boldsymbol{Q}}_j G_{ij}(\widehat{\boldsymbol{x}}) &+ \frac{1}{2}\boldsymbol{E}^T\widehat{\boldsymbol{B}}_{j,f}\left(G_{ij}(\widehat{\boldsymbol{x}}_f) - \boldsymbol{E}G_{ij}(\widehat{\boldsymbol{x}})\right)\\ &+ \frac{1}{2}\boldsymbol{E}^T\widehat{\boldsymbol{B}}_{j,f}\left(\boldsymbol{E}_{fm}G_{ij}(\widehat{\boldsymbol{x}}_m) - \boldsymbol{E}G_{ij}(\widehat{\boldsymbol{x}})\right)\\ &+ \frac{1}{2}\boldsymbol{E}^T\boldsymbol{E}_{mf}^T\widehat{\boldsymbol{B}}_{j,m}\left(G_{ij}(\widehat{\boldsymbol{x}}_m) - \boldsymbol{E}_{mf}G_{ij}(\widehat{\boldsymbol{x}}_f)\right).\end{aligned}$$

where $G_{ij}(\widehat{\boldsymbol{x}}), G_{ij}(\widehat{\boldsymbol{x}}_f), G_{ij}(\widehat{\boldsymbol{x}}_m)$ denote the values of G_{ij} at volume, surface, and mortar points. By the fact that $G_{ij} \in Q^N$ and $\boldsymbol{E}, \boldsymbol{E}_{mf}$ are degree N interpolation operators, the first and third correction terms vanish. The remaining boundary correction terms are

$$\boldsymbol{E}^T\widehat{\boldsymbol{B}}_{j,f}\left(\boldsymbol{E}_{fm}G_{ij}(\widehat{\boldsymbol{x}}_m) - \boldsymbol{E}G_{ij}(\widehat{\boldsymbol{x}})\right). \tag{22}$$

Recall that $\widehat{\boldsymbol{B}}_{i,f}$ is a diagonal matrix whose entries are $\widehat{\boldsymbol{n}}_{i,m}$ scaled by the mortar quadrature weights. On tensor product elements, $\widehat{\boldsymbol{n}}_{i,m} = \pm 1$ on faces where $\widehat{x}_i = \pm 1$ and zero otherwise. Thus, restricting $\widehat{x}_1 = \pm 1$ yields the boundary values of G_{11} on faces where the correction term (22) is non-zero. We can now show that (22) vanishes for $i = j = 1$ (the cases of $i = 2, \ldots, d$ are similar).

1. If D^k is a quadrilateral element, $G_{11} \in Q^{N_{\text{geo}}, N_{\text{geo}}-1}$, and the surface traces of G_{11} are in the 1D trace space $P^{N_{\text{geo}}-1}$.
2. If D^k is a hexahedral element and G_{ij} is constructed using Approach 1 [17], $G_{11} \in Q^{N_{\text{geo}}, N_{\text{geo}}-1, N_{\text{geo}}-1}$, and the surface traces of G_{11} are in the quadrilateral trace space $Q^{N_{\text{geo}}-1, N_{\text{geo}}-1}$.

Since $N_{\text{geo}} \leq N_m + 1$, by Lemma 3 and the assumption that $N_{\text{geo}} \leq \min(N, N_f + 1, N_m + 1)$, $\boldsymbol{E}_{fm}G_{ij}(\widehat{\boldsymbol{x}}_m) = \boldsymbol{E}G_{ij}(\widehat{\boldsymbol{x}})$ and (22) vanishes.

If Approach 1 [16] is used, then surface traces of G_{11} are contained in $Q^{N_{\text{geo}}, N_{\text{geo}}}$. Then, (22) vanishes since $N_{\text{geo}} \leq \min(N, N_f, N_m)$. In both cases, the remaining terms vanish assuming that G_{ij} satisfies the discrete GCL (11). □

An entropy conservative mortar-based formulation on mapped elements is then

$$\boldsymbol{M}\frac{\mathrm{d}\boldsymbol{u}_h}{\mathrm{d}t} + \begin{bmatrix}\boldsymbol{I}\\ \boldsymbol{E}\\ \boldsymbol{E}_{mf}\boldsymbol{E}\end{bmatrix}^T \sum_{i=1}^{d} \left(2\boldsymbol{Q}_{i,m} \circ \boldsymbol{F}_i\right)\mathbf{1} + \boldsymbol{E}^T\boldsymbol{E}_{mf}^T\boldsymbol{B}_{i,m}\left(\boldsymbol{f}_i^* - \boldsymbol{f}_i(\widetilde{\boldsymbol{u}}_m)\right) = 0 \tag{23}$$

$$\widetilde{\boldsymbol{u}} = \begin{bmatrix}\boldsymbol{u}_h\\ \widetilde{\boldsymbol{u}}_f\\ \widetilde{\boldsymbol{u}}_m\end{bmatrix}, \qquad \widetilde{\boldsymbol{u}}_m = \boldsymbol{u}\left(\boldsymbol{E}_{mf}\boldsymbol{E}\boldsymbol{v}(\boldsymbol{u}_h)\right), \qquad \boldsymbol{f}_i^* = \boldsymbol{f}_{i,S}\left(\widetilde{\boldsymbol{u}}_m^+, \widetilde{\boldsymbol{u}}_m\right), \tag{24}$$

where $\boldsymbol{B}_{i,m} = \operatorname{diag}(\boldsymbol{n}_{i,m} \circ \boldsymbol{w}_m)$ is the diagonal matrix whose entries consist of the scaled physical normals. Again, we assume geometric terms on curved elements are

approximated using polynomials, and that the normals are constructed via (10) and polynomial interpolation.

Add proof - include multi-element case. The proof of entropy conservation is algebraically identical to previous proofs, with Lemma 6 used in place of Lemma 2.

5.3 Theoretical comparisons of Lobatto and Gauss nodes

High order entropy stable collocation schemes on tensor product elements most commonly utilize tensor product quadrature rules constructed from $(N+1)$-point Lobatto nodes [4, 5] or $(N+1)$-point Gauss nodes [1]. On non-conforming meshes, the most natural choice of mortar nodes for such collocation schemes is a composite Lobatto or Gauss rule.

Recall that an $(N+1)$-point Lobatto rule is exact for polynomials of degree $(2N-1)$, while an $(N+1)$-point Gauss rule is exact for polynomials of degree $(2N+1)$. On non-conforming quadrilateral meshes, Theorem 6 implies that both Lobatto and Gauss collocation schemes are stable for $N_{\text{geo}} \leq N$, i.e., for isoparametric curved mappings. On non-conforming hexahedral meshes, Theorem 6 implies that Gauss nodes are also stable for $N_{\text{geo}} \leq N$, but that Lobatto nodes are stable only for $N_{\text{geo}} \leq (N-1)$ if Approach 1 [16] is used to compute geometric terms.

We note that the restriction on the degree of the geometric mapping $N_{\text{geo}} \leq (N-1)$ for Lobatto nodes is not necessary on conforming hexahedral meshes. However, the introduction of non-aligned mortar nodes at non-conforming curved interfaces induces this additional restriction. Moreover, this restriction is consistent with Theorem 3 in [23]. One can remove this constraint on the degree of the geometric mapping by using Approach 2 [17] to compute geometric terms. If Approach 2 is used, then Lobatto collocation schemes remain entropy conservative (stable) on curved hexahedral meshes for all $N_{\text{geo}} \leq N$.

Appendix A describes Approach 1 [16] and Approach 2 [17] in more detail, and demonstrates numerically that both approaches achieve similar high order accuracy in approximating geometric terms.

6 A mortar-based implementation

While the formulation (23) is convenient for analysis, it is less convenient to implement. However, using properties of discretization matrices, we can show that the mortar-based formulation (23) is equivalent to a conforming formulation (13) with a modified numerical flux involving face-local correction terms.

First, we reformulate volume terms by incorporating geometric terms into the definition of the flux matrices. Note that $\boldsymbol{Q}_{i,m}$ can alternatively be defined as [5]

$$\boldsymbol{Q}_{i,m} = \sum_{j=1}^{d} \widehat{\boldsymbol{Q}}_{j,m} \circ \{\{\boldsymbol{G}_{ij}\}\}, \qquad \{\{\boldsymbol{G}_{ij}\}\}_{kl} = \frac{1}{2}\left((\boldsymbol{G}_{ij})_k + (\boldsymbol{G}_{ij})_l\right),$$

where k, l are indices over the total number of volume, surface, and mortar points, and $\boldsymbol{G}_{ij}$ is the vector containing values of G_{ij} at volume, surface, and mortar

points. The volume term of (23) can then be rewritten as

$$\begin{bmatrix} \boldsymbol{I} \\ \boldsymbol{E} \\ \boldsymbol{E}_m\boldsymbol{E} \end{bmatrix}^T \sum_{i=1}^{d} \left(2\boldsymbol{Q}_{i,m} \circ \boldsymbol{F}_i\right) \mathbf{1} = \begin{bmatrix} \boldsymbol{I} \\ \boldsymbol{E} \\ \boldsymbol{E}_m\boldsymbol{E} \end{bmatrix}^T \sum_{i=1}^{d} \left(2\widehat{\boldsymbol{Q}}_{i,m} \circ \widehat{\boldsymbol{F}}_i\right) \mathbf{1} \tag{25}$$

$$\widehat{\boldsymbol{F}}_i = \sum_{j=1}^{d} \{\{\boldsymbol{G}_{ij}\}\} \circ \boldsymbol{F}_i.$$

We next decompose $\widehat{\boldsymbol{F}}_i$ into interactions between volume nodes, surface nodes, and mortar nodes

$$\widehat{\boldsymbol{F}}_i = \begin{bmatrix} \widehat{\boldsymbol{F}}_i^{vv} & \widehat{\boldsymbol{F}}_i^{vf} & \widehat{\boldsymbol{F}}_i^{vm} \\ \widehat{\boldsymbol{F}}_i^{fv} & \widehat{\boldsymbol{F}}_i^{ff} & \widehat{\boldsymbol{F}}_i^{fm} \\ \widehat{\boldsymbol{F}}_i^{mv} & \widehat{\boldsymbol{F}}_i^{mf} & \widehat{\boldsymbol{F}}_i^{mm} \end{bmatrix}$$

By expanding out the definition of the mortar-based SBP operator $\widehat{\boldsymbol{Q}}_{i,m}$ and using properties of the matrices $\widehat{\boldsymbol{B}}_{i,m}, \widehat{\boldsymbol{F}}_i$, (25) can be rewritten as

$$\begin{aligned}
&\begin{bmatrix} \boldsymbol{I} \\ \boldsymbol{E} \\ \boldsymbol{E}_{mf}\boldsymbol{E} \end{bmatrix}^T \left(\begin{bmatrix} \widehat{\boldsymbol{Q}}_i - \widehat{\boldsymbol{Q}}_i^T & \boldsymbol{E}^T\widehat{\boldsymbol{B}}_i & \\ -\widehat{\boldsymbol{B}}_i\boldsymbol{E} & & \widehat{\boldsymbol{B}}_i\boldsymbol{E}_{fm} \\ & -\widehat{\boldsymbol{B}}_{i,m}\boldsymbol{E}_{mf} & \end{bmatrix} \circ \widehat{\boldsymbol{F}}_i \right) \mathbf{1} + \boldsymbol{E}^T\boldsymbol{E}_{mf}^T \left(\widehat{\boldsymbol{B}}_{i,m} \circ \widehat{\boldsymbol{F}}_i^{mm}\right) \mathbf{1} \\
&\quad = \begin{bmatrix} \boldsymbol{I} \\ \boldsymbol{E} \end{bmatrix}^T \left(\begin{bmatrix} \widehat{\boldsymbol{Q}}_i - \widehat{\boldsymbol{Q}}_i^T & \boldsymbol{E}^T\widehat{\boldsymbol{B}}_i \\ -\widehat{\boldsymbol{B}}_i\boldsymbol{E} & \widehat{\boldsymbol{B}}_i \end{bmatrix} \circ \widehat{\boldsymbol{F}}_i \right) \mathbf{1} \\
&\qquad + \boldsymbol{E}^T \left(\boldsymbol{E}_{mf}^T \left(\widehat{\boldsymbol{B}}_{i,m} \circ \widehat{\boldsymbol{F}}_i^{mm}\right) \mathbf{1} - \left(\boldsymbol{B}_i \circ \widehat{\boldsymbol{F}}_i^{ff}\right) \mathbf{1} \right) \\
&\qquad + \boldsymbol{E}^T \left(\left(\widehat{\boldsymbol{B}}_i\boldsymbol{E}_{fm}\right) \circ \widehat{\boldsymbol{F}}_i^{fm} \right) \mathbf{1} - \boldsymbol{E}_{mf}^T \left(\left(\widehat{\boldsymbol{B}}_i\boldsymbol{E}_{mf}\right) \circ \widehat{\boldsymbol{F}}_i^{mf} \right) \mathbf{1}.
\end{aligned}$$

The above expressions can be simplified. First, evaluating $\widehat{\boldsymbol{F}}_i^{mm}, \widehat{\boldsymbol{F}}_i^{ff}$ yields

$$\widehat{\boldsymbol{F}}_i^{mm} = \operatorname{diag}\left(\sum_{j=1}^{d} G_{ij}(\widehat{\boldsymbol{x}}_m) \circ \boldsymbol{f}_i(\widetilde{\boldsymbol{u}}_m) \right), \quad \widehat{\boldsymbol{F}}_i^{ff} = \operatorname{diag}\left(\sum_{j=1}^{d} G_{ij}(\widehat{\boldsymbol{x}}_f) \circ \boldsymbol{f}_i(\widetilde{\boldsymbol{u}}_f) \right),$$

Moreover, recall that the physical normals are defined as products of G_{ij} with reference normals (10). Since $\widehat{\boldsymbol{B}}_{i,m}, \widehat{\boldsymbol{B}}_i$ contain scaled normals on the reference element on the diagonal, we can rewrite the correction terms using the physical normal boundary matrices $\boldsymbol{B}_{i,m}, \boldsymbol{B}_i$

$$\begin{aligned}
&\boldsymbol{E}^T \left(\boldsymbol{E}_{mf}^T \left(\widehat{\boldsymbol{B}}_{i,m} \circ \widehat{\boldsymbol{F}}_i^{mm}\right) \mathbf{1} - \left(\boldsymbol{B}_i \circ \widehat{\boldsymbol{F}}_i^{ff}\right) \mathbf{1} \right) \\
&= \boldsymbol{E}^T \left(\boldsymbol{E}_{mf}^T \boldsymbol{B}_{i,m} \boldsymbol{f}_i(\widetilde{\boldsymbol{u}}_m) - \boldsymbol{B}_i \boldsymbol{f}_i(\widetilde{\boldsymbol{u}}_f) \right).
\end{aligned}$$

The remaining correction terms can also be simplified by noting that $\boldsymbol{E}_{fm}$ are block diagonal matrices, with each block corresponding to a face, and that the scaled reference normals (i.e., the diagonal entries of $\widehat{\boldsymbol{B}}_{i,m}, \widehat{\boldsymbol{B}}_i$) are constant over each face. Then, using (10), we can rewrite the final set of correction terms as

$$\begin{aligned}
&\boldsymbol{E}^T \left(\left(\widehat{\boldsymbol{B}}_i\boldsymbol{E}_{fm}\right) \circ \widehat{\boldsymbol{F}}_i^{fm} \right) \mathbf{1} - \boldsymbol{E}_{mf}^T \left(\left(\widehat{\boldsymbol{B}}_{i,m}\boldsymbol{E}_{mf}\right) \circ \widehat{\boldsymbol{F}}_i^{mf} \right) \mathbf{1} \\
&= \boldsymbol{E}^T \left(\boldsymbol{E}_{fm} \circ \boldsymbol{F}_i^{fm} \circ \{\{\boldsymbol{n}_i\}\}_{fm} \right) \mathbf{1} - \boldsymbol{E}_{mf}^T \left(\boldsymbol{E}_{mf} \circ \boldsymbol{F}_i^{mf} \circ \{\{\boldsymbol{n}_i\}\}_{mf} \right) \mathbf{1}
\end{aligned}$$

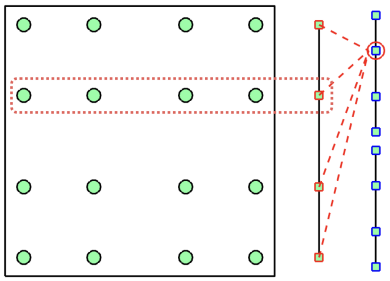

Fig. 3: Coupling between volume, surface, and mortar nodes for formulation (**??**).

where $\boldsymbol{F}_i^{fm} = \left(\boldsymbol{F}_i^{mf}\right)^T$ are the flux matrices whose entries are evaluations of $\boldsymbol{f}_{i,S}$ between solution values at mortar and surface nodes, and $\{\{\boldsymbol{n}_i\}\}_{fm} = \{\{\boldsymbol{n}_i\}\}_{mf}^T$ are matrices whose entries are arithmetic averages of $n_i J_f$ (the ith component of the scaled normal vector) between each mortar and surface point.

Adding these correction terms back into the formulation (23) yields

$$\boldsymbol{M}\frac{\mathrm{d}\boldsymbol{u}_h}{\mathrm{dt}} + \begin{bmatrix}\boldsymbol{I}\\ \boldsymbol{E}\end{bmatrix}^T \sum_{i=1}^{d} \left(2\boldsymbol{Q}_{i,h} \circ \boldsymbol{F}_i\right)\boldsymbol{1} + \boldsymbol{E}^T\left(\boldsymbol{f}_i^* - \boldsymbol{B}_i\boldsymbol{f}_i(\widetilde{\boldsymbol{u}}_f)\right) = 0 \tag{26}$$

$$\boldsymbol{f}_i^* = \boldsymbol{E}_{mf}^T\left(\boldsymbol{B}_{i,m}\boldsymbol{f}_{i,m} + \left(\boldsymbol{E}_{fm} \circ \boldsymbol{F}_i^{fm} \circ \{\{\boldsymbol{n}_i\}\}_{fm} - \boldsymbol{E}_{mf} \circ \boldsymbol{F}_i^{mf} \circ \{\{\boldsymbol{n}_i\}\}_{mf}\right)\boldsymbol{1}\right),$$

where $\boldsymbol{f}_{i,m} = \boldsymbol{f}_{i,S}(\widetilde{\boldsymbol{u}}_m^+, \widetilde{\boldsymbol{u}}_m)$ is the numerical flux computed using the at mortar points. The formulation (26) is nearly equivalent to the hybridized mortar formulation, with the main difference being the presence of skew-symmetric correction terms in the definition of the numerical flux. Note that in this formulation, the only interactions between surface and mortar nodes occur within the computation of $\boldsymbol{f}_i^*$, and involve only computations which are local to mortar interfaces.

Remark 1 If the surface and mortar nodes are the same, then

$$\boldsymbol{E}_{mf} = \boldsymbol{E}_{fm} = \boldsymbol{I}, \qquad \{\{\boldsymbol{n}_i\}\}_{fm} = \{\{\boldsymbol{n}_i\}\}_{mf}$$

and the correction terms in the definition of $\boldsymbol{f}_i^*$ cancel out. The formulation (26) then reverts to a Gauss collocation scheme [2] on conforming meshes.

7 Numerical experiments

7.1 2D results

Figure **??** shows preliminary results for the 2D compressible Euler equations by the PI on a manually constructed non-conforming quadrilateral mesh, with volume, surface, and mortar quadratures constructed from one-dimensional Lobatto or Gauss quadrature rules. The PI has verified that this preliminary implementation of the mortar-based formulation is discretely entropy stable. A preliminary

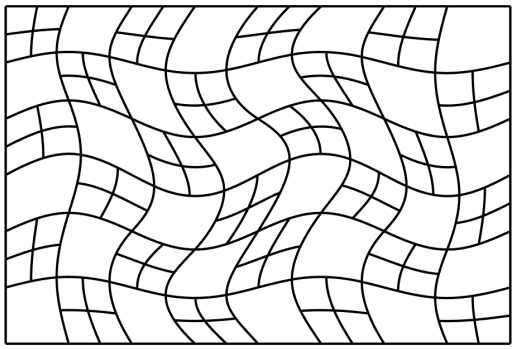

Fig. 4: An $N = 3$ mesh used in the refinement and entropy conservation studies.

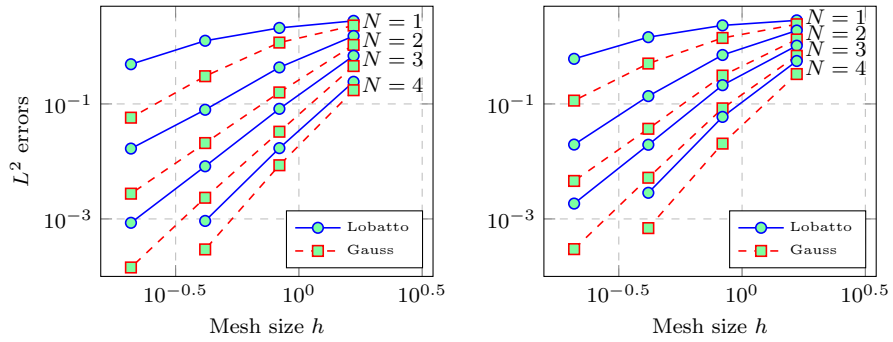

(a) Affine mesh (b) Curved mesh

Fig. 5: Blah

accuracy analysis for the skew-symmetric formulation (**??**) also suggests that Lobatto quadrature should achieve an $O(h^N)$ rate of convergence and that Gauss quadrature should achieve an $O(h^{N+1})$ rate of convergence. Both predicted rates are confirmed in Figure **??**.

Gauss Lobatto quadrature

Gauss quadrature

7.2 3D results

Gauss Lobatto quadrature

Gauss quadrature

8 Conclusions and extensions of the mortar-based approach

Extensions to 3D meshes: double anisotropic mortar for $O(N^3)$ operations vs $O(N^4)$.

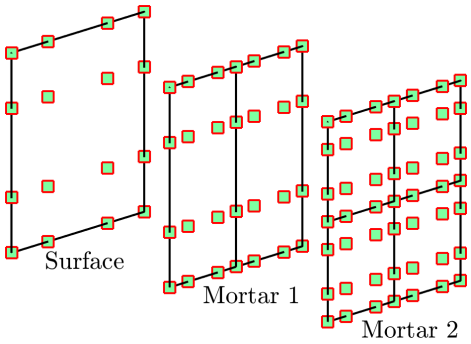

Fig. 6: Two-layer mortars for reduced $O(N^3)$ computational cost on non-conforming hexahedral interfaces.

Extension to p non-conforming meshes is straightforward. Simply replace the definition of a mortar.

Extension to general quadratures just requires replacing $\boldsymbol{I}$ with $\boldsymbol{V}_q, \boldsymbol{P}_q$, and redefining $\boldsymbol{E}$ matrices.

Explain why non-hexahedral elements isn't as much of an issue - Shadpey [24] use this for simplicial elements. The interpolation operators are dense, and using the mortar-based approach wouldn't actually decrease the number of operations.

Jesse Chan gratefully acknowledges support from the National Science Foundation under awards DMS-1719818 and DMS-1712639.

A Geometric terms for curved hexahedral meshes

Entropy conservation (stability) requires that the geometric terms be constructed appropriately. In addition to requiring satisfaction of the discrete geometric conservation law [7, 8, 16], the schemes derived in this work require that the polynomial degree of the geometric terms be related to the accuracy of the surface and mortar quadrature rules. We consider two methods to construct geometric terms: Approach 1 from [16], and Approach 2 from [17].

Entropy conservation (or stability) on non-conforming meshes also require that the scaled outward normals are equal and opposite across each mortar node. This holds if the mesh is *watertight* or *well-constructed*, such that there are no gaps between neighboring elements. Several conditions which guarantee that a curved non-conforming mesh is well-constructed are described in [18]. For the two-dimensional numerical experiments in this work, we construct watertight curved non-conforming meshes by first curving a conforming mesh. We then locally refine certain parent elements and transfer the geometric terms of the parent element to the child elements. For the three-dimensional numerical experiments in this work, finish.

A.1 Construction of geometric terms for curved hexahedra

Let $\boldsymbol{D}_{1\mathrm{D}}$ denote the $(N_{\mathrm{geo}}+1)\times(N_{\mathrm{geo}}+1)$ one-dimensional nodal differentiation matrix at degree N_{geo} Lobatto nodes. Multi-dimensional differentiation matrices on the reference hexahedron can then be constructed via

$$\begin{aligned}\boldsymbol{D}_1 &= \boldsymbol{D}_{1\mathrm{D}} \otimes \boldsymbol{I}_{1\mathrm{D}} \otimes \boldsymbol{I}_{1\mathrm{D}} \\ \boldsymbol{D}_2 &= \boldsymbol{I}_{1\mathrm{D}} \otimes \boldsymbol{D}_{1\mathrm{D}} \otimes \boldsymbol{I}_{1\mathrm{D}} \\ \boldsymbol{D}_3 &= \boldsymbol{I}_{1\mathrm{D}} \otimes \boldsymbol{I}_{1\mathrm{D}} \otimes \boldsymbol{D}_{1\mathrm{D}},\end{aligned}$$

where $\boldsymbol{I}_{1\mathrm{D}}$ is the $(N_{\mathrm{geo}}+1)\times(N_{\mathrm{geo}}+1)$ identity matrix.

Let $\boldsymbol{x},\boldsymbol{y},\boldsymbol{z}$ denote the vectors of physical nodal coordinates of a curved degree N_{geo} element. Approach 1 in [16] constructs scaled geometric terms $G_{ij} = J\frac{\partial \widehat{x}_j}{\partial x_i}$ via

$$\begin{aligned}
\boldsymbol{G}_{i1} &= \alpha_i \left(\boldsymbol{D}_3 \boldsymbol{f}_{i2} - \boldsymbol{D}_2 \boldsymbol{f}_{i3}\right), \\
\boldsymbol{G}_{i2} &= \alpha_i \left(\boldsymbol{D}_1 \boldsymbol{f}_{i3} - \boldsymbol{D}_3 \boldsymbol{f}_{i1}\right), \\
\boldsymbol{G}_{i3} &= \alpha_i \left(\boldsymbol{D}_2 \boldsymbol{f}_{i1} - \boldsymbol{D}_1 \boldsymbol{f}_{i2}\right)
\end{aligned}$$

where $\alpha_1 = 1$ and $\alpha_2 = \alpha_3 = -1$, and the geometric "potentials" $\boldsymbol{f}_{ij}$ are defined as

$$\boldsymbol{f}_{1j} = (\boldsymbol{D}_j \boldsymbol{y}) \circ \boldsymbol{z}, \qquad \boldsymbol{f}_{2j} = (\boldsymbol{D}_j \boldsymbol{x}) \circ \boldsymbol{z}, \qquad \boldsymbol{f}_{3j} = (\boldsymbol{D}_j \boldsymbol{y}) \circ \boldsymbol{x}. \tag{27}$$

The resulting geometric terms are tensor product polynomials of degree $G_{ij} \in Q^{N_{\mathrm{geo}}}$. If $N_{\mathrm{geo}} < N$, we use polynomial interpolation to compute values of the geometric terms at degree N Lobatto nodes.

Approach 2 in [17] (see also [9], Footnote 3) modifies this approach slightly by reducing the degree of each geometric potentials along a coordinate direction. Let $\boldsymbol{I}_{N_{\mathrm{geo}}}^{N_{\mathrm{geo}}-1}$ denote the interpolation operator from degree N_{geo} to degree $N_{\mathrm{geo}}-1$ Lobatto nodes, and let $\boldsymbol{I}_{N_{\mathrm{geo}}-1}^{N_{\mathrm{geo}}}$ denote the interpolation operator from degree $N_{\mathrm{geo}}-1$ to degree N_{geo} Lobatto nodes. Define the degree reduction operator $\boldsymbol{F}_{1\mathrm{D}}$ as the product of these interpolation operators

$$\boldsymbol{F}_{1\mathrm{D}} = \boldsymbol{I}_{N_{\mathrm{geo}}-1}^{N_{\mathrm{geo}}} \boldsymbol{I}_{N_{\mathrm{geo}}}^{N_{\mathrm{geo}}-1}.$$

Multiplication by $\boldsymbol{F}_{1\mathrm{D}}$ lowers the degree of a polynomial from N_{geo} to $N_{\mathrm{geo}}-1$ while leaving the boundary values unchanged. We can define multi-dimensional degree reduction operators

$$\begin{aligned}
\boldsymbol{F}_1 &= \boldsymbol{F}_{1\mathrm{D}} \otimes \boldsymbol{I}_{1\mathrm{D}} \otimes \boldsymbol{I}_{1\mathrm{D}} \\
\boldsymbol{F}_2 &= \boldsymbol{I}_{1\mathrm{D}} \otimes \boldsymbol{F}_{1\mathrm{D}} \otimes \boldsymbol{I}_{1\mathrm{D}} \\
\boldsymbol{F}_3 &= \boldsymbol{I}_{1\mathrm{D}} \otimes \boldsymbol{I}_{1\mathrm{D}} \otimes \boldsymbol{F}_{1\mathrm{D}}.
\end{aligned}$$

Suppose $u \in Q^{N_{\mathrm{geo}}}$ is represented using nodal values $\boldsymbol{u}$; then, $\boldsymbol{F}_1 \boldsymbol{u}$ corresponds to a polynomial in $Q^{N_{\mathrm{geo}}-1,N_{\mathrm{geo}},N_{\mathrm{geo}}}$. In other words, $\boldsymbol{F}_i$ lowers the polynomial degree in the ith coordinate by 1. Approach 2 computes the geometric terms $\boldsymbol{G}_{ij}$ via

$$\begin{aligned}
\boldsymbol{G}_{i1} &= \alpha_i \left(\boldsymbol{D}_3 \widetilde{\boldsymbol{f}}_{i2} - \boldsymbol{D}_2 \widetilde{\boldsymbol{f}}_{i3}\right), \\
\boldsymbol{G}_{i2} &= \alpha_i \left(\boldsymbol{D}_1 \widetilde{\boldsymbol{f}}_{i3} - \boldsymbol{D}_3 \widetilde{\boldsymbol{f}}_{i1}\right), \\
\boldsymbol{G}_{i3} &= \alpha_i \left(\boldsymbol{D}_2 \widetilde{\boldsymbol{f}}_{i1} - \boldsymbol{D}_1 \widetilde{\boldsymbol{f}}_{i2}\right)
\end{aligned}$$

where $\widetilde{\boldsymbol{f}}_{ij} = \boldsymbol{F}_j \boldsymbol{f}_{ij}$ are degree-reduced geometric potentials, and the original geometric potentials $\boldsymbol{f}_{ij}$ are computed via (27). Since multiplication by $\boldsymbol{D}_i$ reduces the degree by 1 in the ith coordinate by 1, the resulting geometric terms G_{ij} satisfy

$$\begin{aligned}
G_{i1} &\in Q^{N_{\mathrm{geo}},N_{\mathrm{geo}}-1,N_{\mathrm{geo}}-1} \\
G_{i2} &\in Q^{N_{\mathrm{geo}}-1,N_{\mathrm{geo}},N_{\mathrm{geo}}-1} \\
G_{i3} &\in Q^{N_{\mathrm{geo}}-1,N_{\mathrm{geo}}-1,N_{\mathrm{geo}}}, \qquad i = 1,2,3.
\end{aligned}$$

While Approach 1 is nominally more accurate than Approach 2, both approaches achieve nearly identical accuracy and convergence rates. We analyze L^2 errors using Approach 1 and Approach 2 by computing exact values of G_{ij} using the cross product formula [16, 25]. We construct a curved mesh by transforming a Cartesian hexahedral grid on $[-1,1]^3$ by interpolating the global curved mapping at Lobatto nodes

$$\begin{aligned}
\widetilde{x} &= x + \frac{1}{4}\cos(x)\sin(y)\sin(z) \\
\widetilde{y} &= y + \frac{1}{4}\sin(x)\cos(y)\sin(z) \\
\widetilde{z} &= z + \frac{1}{4}\sin(x)\sin(y)\cos(z),
\end{aligned}$$

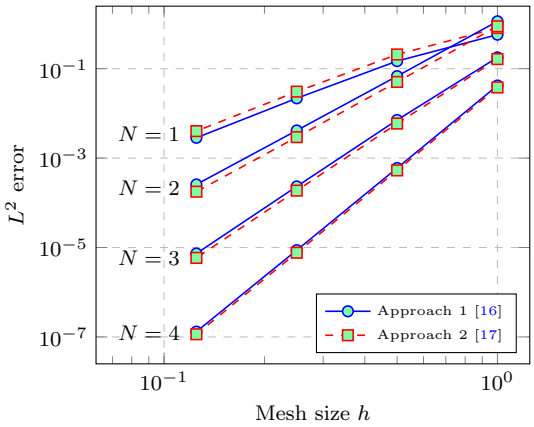

Fig. 7: Blah

N	1	2	3	4
Approach 1	2.8472	4.0772	4.9896	6.0879
Approach 2	2.8494	4.0238	4.9608	6.0769

Table 1: Computed L^2 error convergence rates for Approach 1 [16] and Approach 2 [17]. Both approaches achieve $O(h^{N+2})$ rates, which were proven in [7, 8] for simplicial elements.

where x, y, z denote coordinates on the Cartesian grid and $\widetilde{x}, \widetilde{y}, \widetilde{z}$ denote coordinates on the mapped curved domain. Figure 7 shows the convergence of the L^2 error over all geometric terms under mesh refinement. Table 1 shows computed convergence rates, which match the $O(h^{N+2})$ rates proven in [7, 8] for simplicial elements.

References

1. Jesse Chan, David C Del Rey Fernández, and Mark H Carpenter. Efficient entropy stable Gauss collocation methods. *SIAM Journal on Scientific Computing*, 41(5):A2938–A2966, 2019.
2. Jesse Chan. On discretely entropy conservative and entropy stable discontinuous Galerkin methods. *Journal of Computational Physics*, 362:346 – 374, 2018.
3. Travis C Fisher and Mark H Carpenter. High-order entropy stable finite difference schemes for nonlinear conservation laws: Finite domains. *Journal of Computational Physics*, 252:518–557, 2013.
4. Mark H Carpenter, Travis C Fisher, Eric J Nielsen, and Steven H Frankel. Entropy Stable Spectral Collocation Schemes for the Navier–Stokes Equations: Discontinuous Interfaces. *SIAM Journal on Scientific Computing*, 36(5):B835–B867, 2014.
5. Gregor J Gassner, Andrew R Winters, and David A Kopriva. Split form nodal discontinuous Galerkin schemes with summation-by-parts property for the compressible Euler equations. *Journal of Computational Physics*, 327:39–66, 2016.
6. Tianheng Chen and Chi-Wang Shu. Entropy stable high order discontinuous Galerkin methods with suitable quadrature rules for hyperbolic conservation laws. *Journal of Computational Physics*, 345:427–461, 2017.
7. Jared Crean, Jason E Hicken, David C Del Rey Fernández, David W Zingg, and Mark H Carpenter. Entropy-stable summation-by-parts discretization of the Euler equations on general curved elements. *Journal of Computational Physics*, 356:410–438, 2018.

8. Jesse Chan and Lucas C Wilcox. Discretely entropy stable weight-adjusted discontinuous Galerkin methods on curvilinear meshes. *Journal of Computational Physics*, 378:366 – 393, 2019.
9. Jesse Chan. Skew-Symmetric Entropy Stable Modal Discontinuous Galerkin Formulations. *Journal of Scientific Computing*, 81(1):459–485, Oct 2019.
10. Christine Bernardi, Yvon Maday, and Anthony T Patera. Domain decomposition by the mortar element method. In *Asymptotic and numerical methods for partial differential equations with critical parameters*, pages 269–286. Springer, 1993.
11. Lucas Friedrich, Andrew R Winters, David C Del Rey Fernández, Gregor J Gassner, Matteo Parsani, and Mark H Carpenter. An entropy stable h/p non-conforming discontinuous Galerkin method with the summation-by-parts property. *Journal of Scientific Computing*, pages 1–37.
12. Constantine M Dafermos. *Hyperbolic conservation laws in continuum physics*. Springer, 2005.
13. David C Del Rey Fernández, Pieter D Boom, and David W Zingg. A generalized framework for nodal first derivative summation-by-parts operators. *Journal of Computational Physics*, 266:214–239, 2014.
14. Tianheng Chen and Chi-Wang Shu. Review of entropy stable discontinuous Galerkin methods for systems of conservation laws on unstructured simplex meshes, 2019. Accessed July 25, 2019.
15. PD Thomas and CK Lombard. Geometric conservation law and its application to flow computations on moving grids. *AIAA journal*, 17(10):1030–1037, 1979.
16. David A Kopriva. Metric identities and the discontinuous spectral element method on curvilinear meshes. *Journal of Scientific Computing*, 26(3):301–327, 2006.
17. Jeremy E Kozdon and Lucas C Wilcox. An energy stable approach for discretizing hyperbolic equations with nonconforming discontinuous Galerkin methods. *Journal of Scientific Computing*, 76(3):1742–1784, 2018.
18. David A Kopriva, Florian J Hindenlang, Thomas Bolemann, and Gregor J Gassner. Free-Stream Preservation for Curved Geometrically Non-conforming Discontinuous Galerkin Spectral Elements. *Journal of Scientific Computing*, 79(3):1389–1408, 2019.
19. Eitan Tadmor. The numerical viscosity of entropy stable schemes for systems of conservation laws. I. *Mathematics of Computation*, 49(179):91–103, 1987.
20. Eitan Tadmor and Weigang Zhong. Entropy stable approximations of Navier–Stokes equations with no artificial numerical viscosity. *Journal of Hyperbolic Differential Equations*, 3(03):529–559, 2006.
21. Johnathon Upperman and Nail K Yamaleev. Entropy stable artificial dissipation based on Brenner regularization of the Navier-Stokes equations. *Journal of Computational Physics*, 393:74–91, 2019.
22. Andrew R Winters, Dominik Derigs, Gregor J Gassner, and Stefanie Walch. A uniquely defined entropy stable matrix dissipation operator for high Mach number ideal MHD and compressible Euler simulations. *Journal of Computational Physics*, 332:274–289, 2017.
23. David C Fernandez, Mark H Carpenter, Lisandro Dalcin, Stefano Zampini, and Matteo Parsani. Entropy Stable h/p-Nonconforming Discretization with the Summation-by-Parts Property for the Compressible Euler and Navier-Stokes Equations. *arXiv preprint arXiv:1910.02110*, 2019.
24. Siavosh Shadpey and David W Zingg. Energy-and Entropy-Stable Multidimensional Summation-by-Parts Discretizations on Non-Conforming Grids. In *AIAA Aviation 2019 Forum*, page 3204, 2019.
25. Jan S Hesthaven and Tim Warburton. *Nodal discontinuous Galerkin methods: algorithms, analysis, and applications*, volume 54. Springer, 2007.